

# Icotinib Induces Mechanism-Based Inactivation of Recombinant Human CYP3A4/5 Possibly via Heme Destruction by Ketene Intermediate<sup>§</sup>

Chen Sun,<sup>1</sup> Huimin Zhao,<sup>1</sup> Wei Li, Yudi Jia, Yi Yang, Ying Peng, and Jiang Zheng

*Wuya College of Innovation (C.S., H.Z., W.L., Y.J., Y.Y., Y.P., J.Z.), State Key Laboratory of Functions and Applications of Medicinal Plants, Guizhou Provincial Key Laboratory of Pharmaceutics (J.Z.), and Key Laboratory of Environmental Pollution Monitoring and Disease Control (J.Z.), Ministry of Education, Guizhou Medical University, Guiyang, People's Republic of China; School of Pharmaceutical Engineering, Shenyang Pharmaceutical University, Shenyang, Liaoning, People's Republic of China (J.Z.)*

Received January 13, 2021; accepted July 7, 2021

## ABSTRACT

Icotinib (ICT) is an antitumor drug approved by China National Medical Products Administration and is found to be effective against non-small cell lung cancer. The present study aimed at the interaction of ICT with CYP3A. ICT exhibited time-, concentration-, and NADPH-dependent inhibitory effect on recombinant human CYP3A4/5. About 60% of CYP3A activity was suppressed by ICT at 50  $\mu$ M after 30 minutes. The observed enzyme inhibition could not be recovered by dialysis. Nifedipine protected CYP3A from the inactivation by ICT. The inhibitory effects of ICT on CYP3A were influenced neither by glutathione/*N*-acetyl lysine nor by superoxide dismutase/catalase. Incubation of ICT with human hepatic microsomes produced a ketene reactive intermediate trapped by 4-bromobenzylamine. CYP3A4 dominated the metabolic activation of ICT to the ketene intermediate. Ethyl and vinyl analogs of ICT did not induce inactivation of recombinant human CYP3A4/5, which indicates that acetylenic bioactivation of ICT

contributed to the enzyme inactivation. Moreover, the metabolic activation of ICT resulted in heme destruction. In conclusion, this study demonstrated that ICT was a mechanism-based inactivator of recombinant human CYP3A4/5, and heme destruction by the ketene metabolite may be responsible for the observed CYP3A inactivation.

## SIGNIFICANCE STATEMENT

Cytochrome P450 enzymes play an important role in drug-drug interactions. The present study demonstrated that icotinib, an inhibitor of epidermal growth factor receptor used to treat non-small cell lung cancer, is a mechanism-based inactivator of recombinant human CYP3A4/5. The study provided solid evidence for the involvement of acetylene moiety in the metabolic activation as well as the inactivation of the enzyme. Furthermore, the resulting ketene intermediate was found to destroy heme, which is possibly responsible for the observed enzyme inactivation.

## Introduction

Icotinib (ICT; **1** in Fig. 1) is found to inhibit epidermal growth factor receptor tyrosine kinases (Tan et al., 2012). The progression and apoptosis of tumor cells are reportedly associated with the activity of the tyrosine kinases. These enzymes are often used as antitumor targets for drug development (Ciardiello and Tortora, 2001). Over the last decade, the U.S. Food and Drug Administration has approved several inhibitors of the kinases as antitumor agents against non-small cell lung cancer (NSCLC), such as afatinib, erlotinib, and gefitinib (Campbell et al.,

2010; Keating, 2014; Gridelli et al., 2010). ICT, discovered by Betta Pharmaceuticals Co., Ltd., in China, showed favorable efficacy against NSCLC compared with gefitinib in clinical studies (Ou, 2012; Shi et al., 2013; Gu et al., 2013). In 2011, ICT was granted approval for the treatment of NSCLC by the China National Medical Products Administration.

ICT is extensively metabolized by CYP1A2, 2C19, and 3A4 in human liver, and CYP3A4 (53.48%) mainly contributes to the metabolism of ICT (Chen et al., 2015; Ruan et al., 2012). It is noticeable, however, that patients with NSCLC administered ICT are often treated with other drugs because of various conditions of clinical therapy. For instance, the regimen of ICT in combination with zoledronic acid is used for the treatment of NSCLC with bone metastases (Wang et al., 2017). ICT is combined with rapamycin for the treatment of advanced NSCLC after kidney transplantation (Zhao et al., 2014). Furthermore, ICT is often used together with traditional Chinese medicines in China

<sup>1</sup>C.S. and H. Z. contributed equally to this work.

This work was partially supported by the National Natural Science Foundation of China [Grants 81773813 and 81830104] and the Natural Science Foundation of Liaoning Province of China [Grant 201801561].

<http://dx.doi.org/10.1124/dmd.121.000369>

<sup>§</sup> This article has supplemental material available at [dmd.aspetjournals.org](http://dmd.aspetjournals.org).

**ABBREVIATIONS:** BBA, 4-bromobenzylamine; DDI, drug-drug interaction; DTT, DL-dithiothreitol; GSH, glutathione; HLMS, human liver microsomes; HPLC, high-performance liquid chromatography; ICT, icotinib; IS, internal standard;  $K_{obs}$ , the observed inactivation rate of the affected enzyme; LC, liquid chromatography; LOD, limit of detection; LOQ, limit of quantitation; MBI, mechanism-based inactivation; *m*-CPBA, *m*-chloroperbenzoic acid; MRM, multiple reaction monitoring; MS/MS, tandem mass spectrometry; NAL, *N*-acetyl lysine; NSCLC, non-small cell lung cancer; P450, cytochrome P450; Pd-C, palladium on activated charcoal; ROS, reactive oxygen species; SOD, superoxide dismutase; TFA, trifluoroacetic acid;  $t_R$ , retention time.

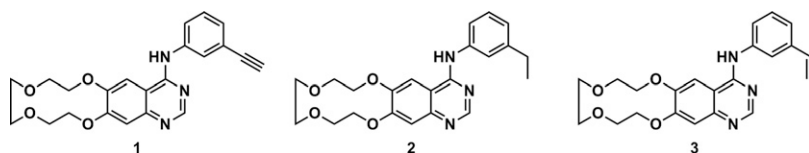


Fig. 1. Chemical structures of compounds employed in the present study.

(Zhao, 2017). These combination therapeutic approaches may result in severe drug-drug interactions (DDIs) often found to result from inhibition of drug-metabolizing enzymes, particularly cytochrome P450 (P450) enzymes (Yamreudeewong et al., 2003).

In the development of pharmaceutical agents, the ability of drug candidates to inhibit P450s needs to be examined for evaluation of DDI potential (Bjornsson et al., 2003; Obach et al., 2005). There are two types of P450 inhibition mechanisms: 1) reversible inhibition and 2) irreversible inhibition. The latter includes affinity labeling and mechanism-based inactivation (MBI). The biochemical basis for MBI generally involves metabolic activation of chemicals to reactive intermediates, which are often electrophiles. Compared with the reversible inhibition, MBI may cause severe clinical safety problems because the generated reactive intermediates can irreversibly inactivate host enzymes via covalent binding of enzyme functional apoprotein or heme (Orr et al., 2012; Hollenberg et al., 2008).

ICT possesses a phenyl terminal acetylene moiety as a hydrophobic group responsible for the recognition of critical amino acids of epidermal growth factor receptor (Stamos et al., 2002). Metabolite identification studies demonstrated that the phenyl terminal acetylene of ICT can be oxidized to the corresponding aryl carboxylic acid (Liu et al., 2011). 7-Ethynylcoumarin, *tert*-butyl acetylene, and 17 $\alpha$ -ethynylestradiol were reported to inactivate CYP2B1, 2E1, and 3A4, respectively (Lin et al., 2002; Blobaum et al., 2002; Regal et al., 2000). These previous studies and structural characteristics led us to propose that ICT may be bio-transformed to electrophilic metabolites, which irreversibly inhibit P450s by modification of the host enzyme.

The time-dependent inhibitory effect of ICT on CYP3A was examined, and the nature of CYP3A inactivation by ICT was determined, according to the criteria for characterization of MBI (Silverman, 1995). The criteria for P450 MBI mainly include 1) time-, concentration-, and NADPH-dependent inhibition; 2) irreversible inhibition; and 3) substrate/competitive inhibitor protection against the time-dependent inhibition. 4-Bromobenzylamine (BBA) capture experiments were also performed to identify potential ketene intermediate of ICT generated. Moreover, we investigated the correlation between the formation of ketene intermediate, heme destruction, and CYP3A inactivation.

## Materials and Methods

**Chemicals and Materials.** ICT ( $\geq 98\%$ ) was provided by Shanghai Ying-Rui-Biopharma Co., Ltd. (Shanghai, China). 6 $\beta$ -Hydroxytestosterone was purchased from Chengdu De-Si-Te Biologic Technology Co., Ltd. (Chengdu, China). Palladium on barium sulfate (10%) and palladium on activated charcoal (Pd-C; 10%) were obtained from Wuhan Zhong-Hua-Yong-Ye Chemical Co., Ltd. (Wuhan, China). 4-Bromobenzylamine was purchased from Beijing Da-Tian-Feng-Tuo Chemical Co., Ltd. (Beijing, China). *m*-Chloroperbenzoic acid (*m*-CPBA) was acquired from Shandong Xiao-Ye Chemical Co., Ltd. (Shandong, China). Quinoline was purchased from Energy Chemical Co., Ltd. (Shanghai, China). Nifedipine and hemin were provided by Dalian Mei-Lun Biotech Co., Ltd. (Dalian, China). Testosterone, propranolol, chrysophanol, *N*-acetylsine, glutathione, superoxide dismutase, catalase, and NADPH were acquired from SolarBio Life Sciences Co., Ltd. (Beijing, China). Iodoacetamide, D, D-thiothreitol (DTT), formic acid, trifluoroacetic acid (TFA), and NH<sub>4</sub>HCO<sub>3</sub> were acquired from Sigma-Aldrich (St. Louis, MO). Mixed male human liver microsomes (HLMs; donor information is listed in Supplemental Table 1) and

recombinant P450 enzymes were purchased from Research Institute for Liver Diseases Co., Ltd. (Shanghai, China). Trypsin and chymotrypsin (sequencing grade) were acquired from Promega Corp. (Madison, WI). BCA protein assay kits were purchased from Beyotime Biotechnology Co., Ltd. (Shanghai, China). Organic solvents were obtained from Merck Life Science Co., Ltd. (Shanghai, China).

**Synthesis.** *N*-(3-Ethylphenyl)-7,8,10,11,13,14-hexahydro-[1,4,7,10]tetraoxacyclododecino[2,3-*g*]quinazolin-4-amine (analog 2). Synthesis of analog 2 (Fig. 1) was conducted by catalytic hydrogenation of ICT. ICT (90 mg, 0.23 mmol) dissolved in 10 ml methanol was mixed with Pd-C (50 mg) in a hydrogen-purged flask. The mixture was stirred for 2.5 hours at room temperature and then submitted to a silica gel column eluted with a mixture of CH<sub>2</sub>Cl<sub>2</sub> and methanol (20:1, v/v) offering 85 mg (95% in yield) of analog 2 (white solid). The product was characterized by <sup>1</sup>H NMR, tandem mass spectrometry (MS/MS), and high-performance liquid chromatography (HPLC)-UV (Supplemental Fig. 1; Supplemental Fig. 2). Electrospray ionization mass spectrometry of C<sub>22</sub>H<sub>25</sub>N<sub>3</sub>O<sub>4</sub>: *m/z* 396.1 [M + H]<sup>+</sup>. HPLC purity: retention time (t<sub>R</sub>) = 5.44 minutes (97.9%). <sup>1</sup>H NMR (600 MHz, DMSO-*d*<sub>6</sub>):  $\delta$ 9.41 (s, 1H), 8.47 (s, 1H), 8.15 (s, 1H), 7.61 (s, 1H), 7.31 (s, 1H), 6.96–7.73 (m, 3H), 4.29–4.31 (m, 4H), 3.76–3.80 (m, 4H), 3.64 (m, 4H), 2.62–2.65 (m, 4H), 1.21–1.24 (t, 3H).

*N*-(3-Vinylphenyl)-7,8,10,11,13,14-hexahydro-[1,4,7,10]tetraoxacyclododecino[2,3-*g*]quinazolin-4-amine (analog 3). A similar procedure was followed as above for the preparation of analog 2 (Fig. 1) for the employment of palladium on barium sulfate (20 mg) in place of Pd-C. Moreover, the activity of the reaction was quenched by adding quinoline (0.5 ml). After 1.5-hour reaction, the resulting mixture was submitted to a silica gel column for purification, which offered 37 mg of analog 3 (41% yield, white solid), followed by characterization using <sup>1</sup>H NMR and MS/MS (Supplemental Figs. 3 and 4). Electrospray ionization mass spectrometry of C<sub>22</sub>H<sub>23</sub>N<sub>3</sub>O<sub>4</sub>: *m/z* 394.1 [M + H]<sup>+</sup>. HPLC purity: t<sub>R</sub> = 4.47 minutes (96.5%). <sup>1</sup>H NMR (600 MHz, DMSO-*d*<sub>6</sub>):  $\delta$ 9.60 (s, 1H), 8.48 (s, 1H), 8.22 (s, 1H), 7.90 (s, 1H), 7.23 (s, 1H), 7.21–7.83 (m, 3H), 6.73–6.76 (dd, 1H), 5.82–5.85 (d, 1H), 5.28–5.30 (d, 1H), 4.29–4.30 (m, 4H), 3.74–3.79 (m, 4H), 3.63 (m, 4H).

*N*-(4-Bromobenzyl)-2-(3-((7,8,10,11,13,14-hexahydro-[1,4,7,10]tetraoxacyclododecino[2,3-*g*]quinazolin-4-yl)amino)phenyl)acetamide (ICT-BBA adduct 5; Fig. 5). As the initial step, the terminal acetylene was oxidized by *m*-CPBA, according to a method reported by McDonald and Schwab (1964), and the resulting product generated in situ reacted with BBA. Briefly, ICT (5.0 mg), *m*-CPBA (50 mg), and BBA (25 mg) were dissolved in 10 ml CH<sub>2</sub>Cl<sub>2</sub>, stirred at 25°C for 12 hours, concentrated under a nitrogen stream, reconstituted in 10% acetonitrile in water, and analyzed by liquid chromatography (LC)-MS/MS.

**Testosterone 6 $\beta$ -Hydroxylation Assay.** Reactions were composed of primary and secondary incubations. The primary mixture contained ICT (0 or 50  $\mu$ M), HLMs (0.5 mg protein/ml), and MgCl<sub>2</sub> (3.2 mM) in 200  $\mu$ l PBS (100 mM, pH 7.4) with 0.5% organic solvent. The primary mixture was preincubated at 37°C for 3 minutes, followed by adding NADPH (1.0 mM) to launch the reaction. The mixture was incubated for 0, 10, 20, or 30 minutes, withdrawn (40  $\mu$ l), and mixed with the secondary incubation solution. The secondary incubation mixture contained MgCl<sub>2</sub> (3.2 mM), testosterone (200  $\mu$ M), and NADPH (1.0 mM) in 120  $\mu$ l PBS. After 15-minute incubation, ice-cold acetonitrile (equal volume) was incorporated to terminate the reaction. The precipitation reagent contained propranolol (500 ng/ml) as an internal standard. The supernatants were submitted to LC-MS/MS for analysis of 6 $\beta$ -hydroxytestosterone and propranolol after centrifugation at 19,000g for 10 minutes.

To evaluate the feasibility of the method, selectivity, limit of detection (LOD), limit of quantitation (LOQ), linearity, precision, accuracy, matrix effect, and stability were determined as inspired by previous literature (Foo et al., 2015). An aliquot (40  $\mu$ l) of analysis solutions containing 6 $\beta$ -hydroxytestosterone (concentrations: 0.3, 0.75, 1.5, 3.0, 4.5, and 6.0  $\mu$ g/ml) freshly prepared in methanol from a stock solution (1.0 mg/ml in methanol) was mixed with the pre-prepared

incubation solution (120  $\mu$ l) excluding testosterone, boiled HLMs, or NADPH. The resulting mixtures were handled using the same protocol as described above (final concentrations for LC-MS/MS analysis: 10, 25, 50, 100, 150, and 200 ng/ml). The stability of analytes was determined under two storage conditions (25°C in 12 hours and -4°C in 48 hours) based on the needs of the experiments.

**Determination of Time-, Concentration-, and NADPH-Dependent Inhibition of CYP3A by ICT.** The primary mixture contained HLMs (0.5 mg protein/ml), MgCl<sub>2</sub> (3.2 mM), and ICT at concentrations of 0, 5, 15, 25, 35, or 50  $\mu$ M in 200  $\mu$ l PBS. The mixture was preincubated for 3 minutes at 37°C, followed by adding NADPH (1.0 mM) to launch the reactions. In a separate experiment, the incubation reaction received the same volume of PBS in place of NADPH to determine NADPH dependency of the enzyme inhibition. The mixture was incubated for 0, 10, 20, and 30 minutes, withdrawn (40  $\mu$ l), and mixed with the secondary incubation solution. The secondary incubation mixture contained MgCl<sub>2</sub> (3.2 mM), NADPH (1.0 mM), and testosterone (200  $\mu$ M) in 120  $\mu$ l PBS. After 15-minute incubation, ice-cold acetonitrile (equal volume) containing propranolol [500 ng/ml, internal standard (IS)] was incorporated to terminate the reaction. Samples were then prepared and analyzed as stated above.

**Examination of Effect of Substrate Protection.** The primary incubation mixture contained ICT (50  $\mu$ M), nifedipine (100  $\mu$ M, a substrate of CYP3A), HLMs (0.5 mg protein/ml), and MgCl<sub>2</sub> (3.2 mM) in 200  $\mu$ l PBS. The reaction was launched by incorporation of NADPH (1.0 mM). The mixture was incubated for 0, 10, 20, and 30 minutes, withdrawn (40  $\mu$ l), and mixed with the secondary incubation solution. The contents of the secondary incubation mixture and sample preparation for analysis were the same as described above. The primary incubations, which lacked ICT or/and nifedipine, were used as the corresponding control groups.

**Examination of Effects of *N*-Acetyl Lysine/Glutathione or Superoxide Dismutase/Catalase on Inhibition of CYP3A.** The primary incubation contained ICT (50  $\mu$ M), HLMs (0.5 mg protein/ml), glutathione (GSH)/*N*-acetyl lysine (NAL) (2.0 mM for each), or superoxide dismutase (SOD)/catalase (800 unit/ml for each) and MgCl<sub>2</sub> (3.2 mM) in 200  $\mu$ l PBS. The reactions were launched by spiking with NADPH (1.0 mM), followed by incubating for 0, 10, 20, and 30 minutes. The resulting mixtures (40  $\mu$ l) were withdrawn and mixed with the secondary incubation solution. The content of the secondary incubation mixture and sample preparation for analysis were the same as described above.

**Determination of Partition Ratio.** The primary incubation included recombinant human CYP3A4 or CYP3A5 (100 nM for each), ICT (0, 3.125, 6.25, 12.5, 25, 50, 75, 100, or 200  $\mu$ M), and MgCl<sub>2</sub> (3.2 mM) in 100  $\mu$ l PBS. The reactions were launched by spiking with NADPH (1.0 mM). After 0- or 30-minute incubation, a 40  $\mu$ l aliquot of the primary incubation solution was mixed with the secondary incubation solution. The content of the secondary incubation and sample preparation for analysis were as stated above.

**Determination of Inhibition Reversibility.** The primary incubation mixture contained ICT (50  $\mu$ M), HLMs (0.5 mg protein/ml), and MgCl<sub>2</sub> (3.2 mM) in 200  $\mu$ l PBS. The reaction was launched with NADPH (1.0 mM). After 0- or 30-minute incubation, the vehicle- and ICT-treated samples were dialyzed (molecular weight cutoff: 3500 Da) in a PBS solution (1 L) at 4°C. The buffer was changed every 2 hours three times. In parallel, the nondialyzed control and inactivation samples were stored under the same cool condition during the dialysis process. All samples were mixed with the secondary incubation mixture. The content of the secondary incubation and sample preparation for analysis were the same as described above.

**CYP3A Activity Assessment.** The remaining enzyme activity of CYP3A was assessed by monitoring the formation of metabolite 6 $\beta$ -hydroxytestosterone from probe substrate testosterone by LC-MS/MS. An Agilent 1260 HPLC system (Agilent Technologies, Santa Clara, CA) inlined with an AB 5500 triple quadrupole mass spectrometry (SCIEX, Foster City, CA) was used for metabolite assessment. Metabolite responsible for CYP3A (*m/z* 305 $\rightarrow$ 269) was assessed by LC-MS/MS in a positive mode, and propranolol (*m/z* 261 $\rightarrow$ 116) was selected as internal standard in a positive mode, respectively. Chromatographic separation was achieved on a ZORBAX C<sub>18</sub> column (5.0  $\mu$ m, 150 mm  $\times$  4.6 mm; Agilent Technologies, Santa Clara, CA) eluted with mobile phases consisting of acetonitrile and water, which contain 0.1% formic acid. The gradient parameters for the determination of the metabolite related to CYP3A are listed in Supplemental Table 2.

**Ketene Reactive Intermediate Trapping by BBA.** A microsomal incubation mixture contained ICT (50  $\mu$ M), HLMs (0.5 mg protein/ml), BBA (trapping

agent, 5.0 mM), and MgCl<sub>2</sub> (3.2 mM) in 200  $\mu$ l PBS. NADPH (final concentration: 1.0 mM) was spiked to launch the reaction, whereas the control group lacked NADPH. After 30-minute incubation at 37°C, ice-cold acetonitrile (equal volume) was incorporated to terminate the reaction, followed by centrifugation at 19,000g for 10 minutes. The resulting supernatants were subjected to analysis by LC-MS/MS. The formation of ICT-BBA adducts was monitored by scanning of precursor ion *m/z* 169 and 171 as well as ion pairs *m/z* 593 $\rightarrow$ 479 and 595 $\rightarrow$ 481 in a positive mode. In addition, tandem mass spectra of the detected adducts were acquired in an enhanced product ion mode. HPLC separation was achieved on the ZORBAX C<sub>18</sub> column eluted with a mobile system consisting of acetonitrile and water with 0.1% formic acid. The protocol for gradient elution is shown in Supplemental Table 3.

**Comparison of Inactivation Effect of ICT, Analog 2, and Analog 3 on CYP3A.** The primary incubation mixture contained ICT, analog 2, or analog 3 (50  $\mu$ M for each), HLMs (0.5 mg protein/ml), and MgCl<sub>2</sub> (3.2 mM) in 200  $\mu$ l PBS. NADPH (1.0 mM) was incorporated to launch the reaction. The control group received vehicle instead of ICT, analog 2, or analog 3. The primary mixture was incubated at 37°C for 0, 10, 20, or 30 minutes, followed by mixing (40  $\mu$ l aliquots) with the secondary incubation mixture. The content of the secondary incubation mixture and sample preparation for analysis were the same as described above.

**Recombinant Human P450 Incubations.** ICT (50  $\mu$ M), NADPH (1.0 mM), and individual recombinant human P450 enzymes, such as CYP3A5, 3A4, 2E1, 2D6, 2C19, 2C9, 2B6, 2A6, and 1A2 (100 nM), were mixed and incubated at 37°C for 30 minutes. The reaction was stopped by ice-cold acetonitrile (equal volume), which contains propranolol (500 ng/ml, IS).

**Determination of Heme Damage.** A recombinant enzyme incubation mixture contained ICT (50  $\mu$ M), CYP3A4 (100 nM), and MgCl<sub>2</sub> (3.2 mM) in 100  $\mu$ l PBS. To launch the reaction, the incubation mixture received NADPH at a final concentration of 1.0 mM, whereas the control incubation lacked NADPH. After incubating at 37°C for 30 minutes, the resulting mixture was extracted with ten volumes of butanone containing 0.1% TFA and 2.5 ng/ml propranolol (IS). The resulting organic phase was concentrated by blowing with N<sub>2</sub> to dryness and reconstituted in methanol (200  $\mu$ l). After filtration through a 0.22  $\mu$ m membrane, the resulting filtrates were analyzed by LC-MS/MS. Detection of heme and propranolol was achieved by monitoring *m/z* 616 $\rightarrow$ 557 and 260 $\rightarrow$ 116 in a positive ion mode. HPLC separation was performed on the ZORBAX C<sub>18</sub> column. The column was eluted with water and methanol, which contained 0.1% formic acid as shown in Supplemental Table 4. Tandem mass spectrum of heme was acquired in a mode of enhanced product ion.

**Proteomic Analysis of CYP3A4 Apoprotein after Exposure to ICT.** Inactivation of CYP3A4 by ICT (50  $\mu$ M) was performed as described above. The resulting inactivated recombinant CYP3A4 was dialyzed (molecular weight cutoff: 3500 Da) at 4°C in PBS buffer (1 L, 100 mM, pH 7.4) for 6 hours (2 hours three times). Protein contents were assessed by a BCA protein assay kit. The protein samples were separated on SDS-PAGE (15%) according to the general procedure. After 1 hour of discoloring and rehydrating at 60°C in a 50 mM ammonium bicarbonate solution containing 10 mM DTT, the gel responsible for CYP3A4 was sliced and discolored with 50% acetonitrile in a 50 mM NH<sub>4</sub>HCO<sub>3</sub> solution for approximately 30 minutes to make sure that the micelles were colorless. The resulting micelles were placed in 100  $\mu$ l acetonitrile and allowed to stand at 25°C for 30 minutes. The resulting aggregated micelles were mixed with 10 mM DTT dissolved in a 50 mM NH<sub>4</sub>HCO<sub>3</sub> solution (100  $\mu$ l) and stirred at 56°C for 1 hour. The resultant incubation was mixed with 50 mM iodoacetamide dissolved in 50 mM NH<sub>4</sub>HCO<sub>3</sub> (100  $\mu$ l) and was allowed to stand at 25°C in the dark for 60 minutes. The resultant micelles were placed in 100  $\mu$ l acetonitrile, allowed to stand for 30 minutes, and incubated with trypsin (15 ng/ $\mu$ l) in 50 mM NH<sub>4</sub>HCO<sub>3</sub> or chymotrypsin (25 ng/ $\mu$ l) in 10  $\mu$ l Tris-HCl (pH 8.0, 100 mM) digestion solution at 37°C for 16 hours. The resultant micelles were mixed with 50% acetonitrile in water (100  $\mu$ l) containing 5% TFA, placed at 37°C for 1 hour for peptide extraction, and lyophilized to near dryness, followed by mixing with 10  $\mu$ l 0.1% formic acid and LC-MS/MS analysis. Sample analyses were conducted on a Q Exactive Hybrid Quadrupole-Orbitrap Mass Spectrometer (Thermo Fisher Scientific, San Jose, CA) interfaced with an Ultimate 3000 Nanoflow UPLC System (ThermoFisher Scientific). Analyte separation was achieved on a ReproSil-Pur C<sub>18</sub>-AQ resin column (1.9  $\mu$ m, 150  $\mu$ m  $\times$  15 cm, 100 Å) provided by Dr. Maisch (Ammerbuch, Germany). The column was eluted with water and acetonitrile, which contained 0.1% formic acid. The

gradient protocol for eluting of the peptides is shown in Supplemental Table 5. The analysis of raw MS files and target protein identification were achieved via searching a target protein database by MaxQuant (version 1.6.2.10).

**Statistical Analysis.** All of the data reported represent means  $\pm$  S.D. All quantitative experiments were independently repeated three times, and the results were averaged.

## Results

**Methodology Validation.** Incubation mixtures containing boiled microsomes in the absence of  $6\beta$ -hydroxytestosterone and the IS were analyzed by LC-MS/MS. No peaks responsible for  $m/z$  305 $\rightarrow$ 269 and 261 $\rightarrow$ 116 were observed (Supplemental Fig. 5), indicating that no matrix interference was involved and that the analysis was highly selective. The LOD and LOQ of  $6\beta$ -hydroxytestosterone were found to be 2.5 ng/ml (signal-to-noise ratio = 3.9) and 10 ng/ml, respectively. A six-point calibration curve (final concentration range: 10–200 ng/ml) was established and assessed with a correlation coefficient of  $\geq 0.99$ , precision of  $\pm 15\%$ , and accuracy of  $\pm 15\%$ , which is all acceptable. In samples containing  $6\beta$ -hydroxytestosterone at concentrations of 12.5 (low), 75.0 (medium), or 175 ng/ml (high) for the determination of lower LOQ (10 ng/ml) and quality control, the intraday ( $n = 6$ ) and interday ( $n = 3$ ) relative S.D. values of the analyte were less than 12.8%, and the accuracy was 91.5%–111.1% of the nominal value, indicating that the LC-MS/MS method is reliable and reproducible. The matrix effect, obtained from comparison of samples containing boiled HLMs with those lacking boiled HLMs, ranged from 98.2% to 103.6% in quality control samples ( $n = 6$ ). Clearly, no significant matrix effect was observed in response to  $6\beta$ -hydroxytestosterone. Moreover, we examined the stability of the incubation mixtures under the various storage conditions that might be applied to the experiments. Samples were stable at 25°C in 12 hours and 4°C in 48 hours. All methodological data are shown in Supplemental Table 6.

**Screening of Time-Dependent Inhibition of CYP3A by ICT.** ICT (0 and 50  $\mu$ M) was incubated with human hepatic microsomes, followed by examining the remaining activity of CYP3A. Incubation of human liver microsomes with ICT at 50  $\mu$ M for 30 minutes resulted in a significant loss ( $>50\%$ ) of CYP3A activity (Supplemental Fig. 6). This led us to speculate that ICT may be an MBI of CYP3A.

**Time-, Concentration-, and NADPH-Dependent Inhibition of CYP3A by ICT.** Comprehensive enzymatic kinetics were performed to examine time-, concentration-, and NADPH dependency of ICT-induced CYP3A inhibition. Determination of  $6\beta$ -hydroxytestosterone formed in the secondary incubation fortified with testosterone was carried out to assess the resulting activity of remaining CYP3A. The remaining enzyme activity of the incubation mixture of each concentration at 0 minutes was normalized to 100%. Decreased CYP3A activity was observed in microsomal incubation with ICT in a time-dependent manner (Fig. 2A). Additionally, the higher the ICT concentration that was applied in the incubation, the faster the enzyme was inhibited. About 56% of CYP3A activity was suppressed by ICT (50  $\mu$ M) after 30-minute incubation at 37°C. Kinetic constants the maximal rate constant for enzyme inactivation ( $k_{\text{inact}}$ ) and the apparent inactivator concentration displaying half-maximal rate of inactivation ( $K_I$ ) were estimated using Wilson's plot established by plotting of reciprocal of the observed inactivation rate of the affected enzyme ( $K_{\text{obs}}$ ) acquired versus reciprocal ICT concentrations (Fig. 2B). The values of  $k_{\text{inact}}$  and  $K_I$  were found to be 0.013  $\text{minute}^{-1}$  and 20.8  $\mu$ M, respectively. In addition, ICT failed to show such time-dependent inhibition in NADPH-free incubations (Fig. 2C). This suggests the involvement of metabolism in the observed CYP3A inhibition.

**Substrate Protection.** Nifedipine, a substrate of CYP3A, was used to evaluate substrate protection against the enzyme inactivation induced by ICT. Around 47% of CYP3A activity remained after 30-minute incubation with ICT alone (50  $\mu$ M) at 37°C. However, in parallel, the remaining CYP3A activity was found to be about 80% in the

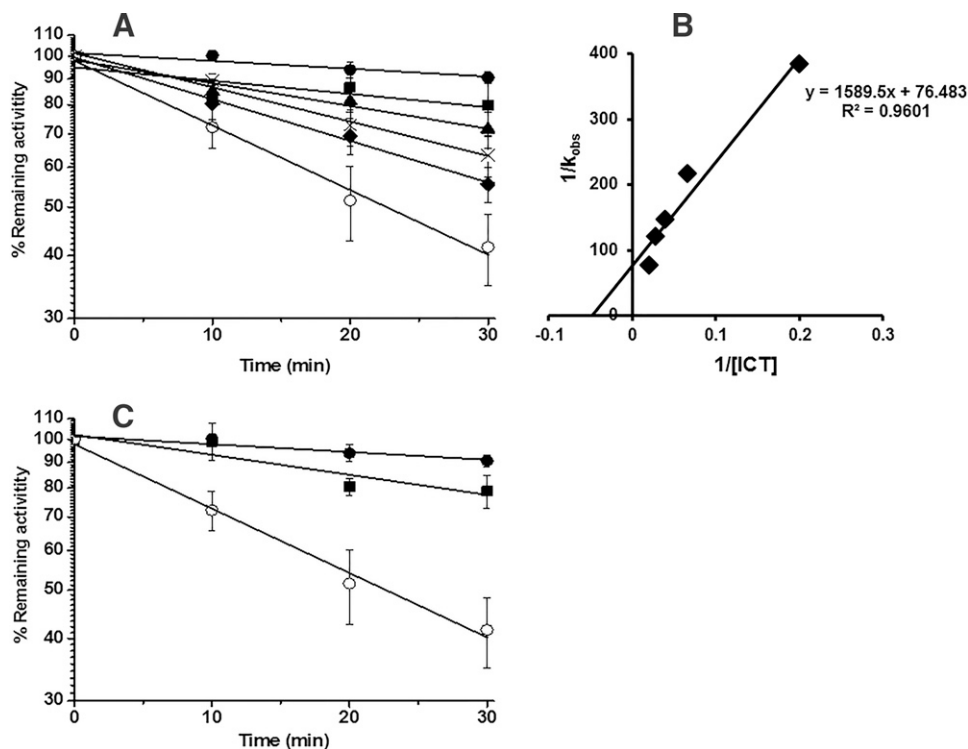


**Fig. 2.** Time-, concentration-, and NADPH-dependent inhibition of CYP3A by ICT (A). Human hepatic microsomal incubations containing ICT at concentrations of 0 ( $\bullet$ ), 5 ( $\blacksquare$ ), 15 ( $\blacklozenge$ ), 25 ( $\times$ ), 35 ( $\blacktriangle$ ), and 50  $\mu$ M ( $\circ$ ) supplemented with NADPH were conducted for 0, 10, 20, and 30 minutes at 37°C and then submitted to CYP3A activity measurement. (B) Wilson's plot. The estimation of  $K_{\text{obs}}$  was achieved by calculation of the slope of the regression lines as (A) indicates. (C) NADPH-dependent inhibition of CYP3A by ICT. Human liver microsomes mixed with ICT at concentrations of 0 ( $\bullet$ ) or 50  $\mu$ M without ( $\blacksquare$ ) or with ( $\circ$ ) NADPH were incubated at 37°C for various time periods and then submitted to CYP3A activity measurement. Data represent means  $\pm$  S.D. ( $n = 3$ ).

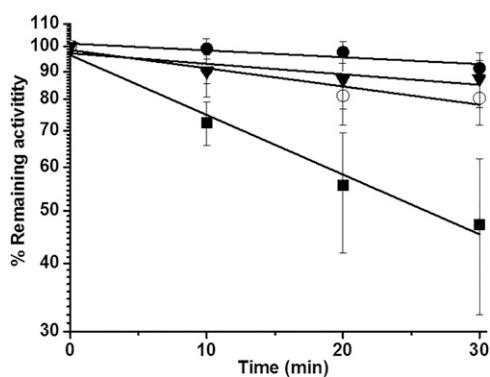


**Fig. 3.** Protection of CYP3A by nifedipine from ICT-induced inactivation. NADPH-fortified human liver microsomes were incubated with ICT (50  $\mu$ M) + nifedipine (○, 100  $\mu$ M), ICT alone (■), nifedipine alone (●), or vehicle (●) for 0, 10, 20, and 30 minutes at 37°C and then submitted to CYP3A activity measurement. Data represent means  $\pm$  S.D. ( $n = 3$ ).

microsomal incubation fortified with nifedipine (Fig. 3). Clearly, nifedipine slowed down the CYP3A inactivation caused by ICT, indicating that bioactivation of ICT occurred in the active site of CYP3A.

**SOD/Catalase Effects on Enzyme Inactivation.** P450-catalyzed reactions could produce reactive oxygen species (ROS). The resulting ROS, such as hydrogen peroxide and superoxide radical anion, could induce the inactivation of the host enzymes. Catalase and SOD, known as ROS scavengers, were included in ICT-fortified microsomal incubations to determine possible roles of ROS in the observed CYP3A inactivation. The presence of the two ROS scavengers revealed little protective effects on ICT-induced CYP3A inactivation (Table 1). This enables us to exclude the involvement of hydrogen peroxide and/or superoxide that may lead to autoinactivation even if ROS were formed during the metabolic process of ICT.

**GSH/NAL Effects on Enzyme Inactivation.** GSH and NAL were fortified in ICT microsomal incubations to determine the protection of exogenous nucleophiles against the CYP3A inactivation. It appears that the two nucleophilic agents failed to offer protection against the inactivation of CYP3A induced by ICT (Table 1). This suggests that reactive intermediates of ICT inactivated the CYP3A prior to leaving the enzyme active site.

**Partition Ratio.** Partition ratio ( $P$  value) stands for the numbers of molecules of the metabolite required for the inactivation of the targeting enzyme.  $P$  value was measured to evaluate the efficiency of ICT on the inactivation of recombinant human CYP3A4/5. The value was estimated by plotting of the percentage of residue activity versus molar ratio of ICT/CYP3A4 or ICT/CYP3A5, according to a published method (Silverman, 1995). ICT at the ICT/CYP3A4 molar ratio above

**Fig. 4.** Loss of CYP3A4 (A) and CYP3A5 (B) activity as a function of the [ICT]/[CYP3A4] or [ICT]/[CYP3A5] molar ratio. The incubation mixture contained recombinant CYP3A4 or CYP3A5 and ICT at concentrations of 0, 3.125, 6.25, 12.5, 25, 50, 75, 100, or 200  $\mu$ M. Data represent means  $\pm$  S.D. ( $n = 3$ ).  $P + 1$  value was estimated by extrapolation from the point of intersection to the abscissa.

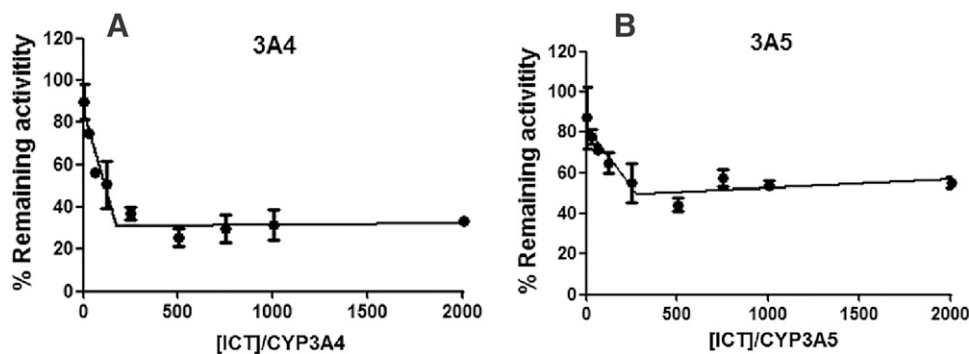


TABLE 1

Protective roles of SOD/catalase and NAL/GSH in CYP3A inhibition induced by ICT

	Remaining activity (%)
ICT	38.1 $\pm$ 4.4
ICT + SOD/catalase	32.4 $\pm$ 2.2
ICT + GSH/NAL	40.5 $\pm$ 6.3

500 inactivated CYP3A4 about 74% (Fig. 4A) and did not further inactivate the enzyme, whereas ICT inactivated CYP3A5 about 55% (Fig. 4B). Meanwhile, turnover numbers ( $P + 1$ ) for CYP3A4 and CYP3A5 were 174 and 277, respectively. Thus  $P$  values were 173 and 276, respectively. Reported  $P$  values for MBI of P450s are in the range of 3 (highly efficient inactivators) to >1000 (inefficient) (Kent et al., 2001). Thus, ICT may be considered to be a moderately efficient inactivator of CYP3A.

**Irreversibility of Inhibition.** Irreversibility of the observed inhibition was probed by exhaustive dialysis of ICT-exposed HLMs. The remaining CYP3A activity of dialyzed sample pretreated with ICT was 39.3  $\pm$  8.3%, whereas that of nondialyzed samples was 35.5  $\pm$  6.1%. This indicates that ICT irreversibly inhibited CYP3A and that the inhibited CYP3A activity could not be recovered by dialysis.

**Generation of Ketene Reactive Intermediate.** We speculated that ICT may be metabolized to ketene intermediate **4** (Fig. 5) and then decided to trap the intermediate using BBA. The generation of the corresponding adduct was determined by LC-MS/MS in a multiple reaction monitoring (MRM) model (ion pairs scanned:  $m/z$  593 $\rightarrow$ 479 and 595 $\rightarrow$ 481). A peak with retention time at 10.9 minutes was observed in ICT-fortified microsomes in the presence of NADPH (Figs. 6C and 6D). We failed to detect such a peak in NADPH-free incubations (Figs. 6A and 6B). The observation of  $m/z$  593 and 595 (molecular ions) enabled us to propose the structure of ICT-BBA adduct **5** (Fig. 5). The observed representative fragments  $m/z$  169, 171, 479, and 481 are possibly responsible for bromobenzyl and quinazoline phenyl portions, respectively. Fragments  $m/z$  294 and 266 may arise from the loss of BBA with and without a carbonyl part (Fig. 6E and Fig. 6F).

Biomimetic synthesis was conducted to verify the proposed structure of ICT-BBA adduct **5**. The terminal acetylene of ICT was oxidized by *m*-CPBA, reacted with BBA, and analyzed by LC-MS/MS. A product in the synthetic sample showed similar  $t_R$  (Fig. 7A and Fig. 7C) and MS/MS fragment patterns (Figs. 7B and 7D) as those detected in microsomal incubation mixtures.

**Role of Acetylenic Moiety in Inactivation of CYP3A by ICT.** ICT analogs **2** and **3** (Fig. 1) were designed and synthesized to determine the functional group responsible for the metabolic activation. As expected, analogs **2** and **3** failed to show time-dependent inhibition of

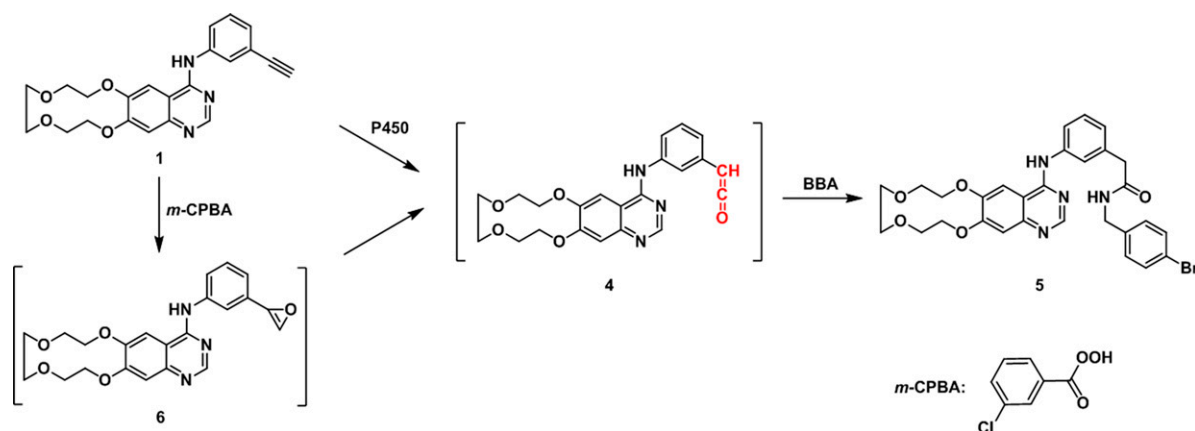


Fig. 5. Biomimetic chemical synthesis of ICT-BBA adduct 5 and proposed bioactivation pathway for the formation of ICT-BBA adduct 5.

CYP3A (Fig. 8). This indicates that the acetylenic moiety played an essential role in ICT-induced CYP3A inactivation, which further supports the proposed involvement of the ketene reactive intermediate in the inactivation of CYP3A by ICT.

**P450 Enzymes Participating in Bioactivation of ICT.** ICT was incubated with a selection of individual recombinant human P450 enzymes. Relative contributions of P450 enzymes to the bioactivation of ICT were determined by monitoring the

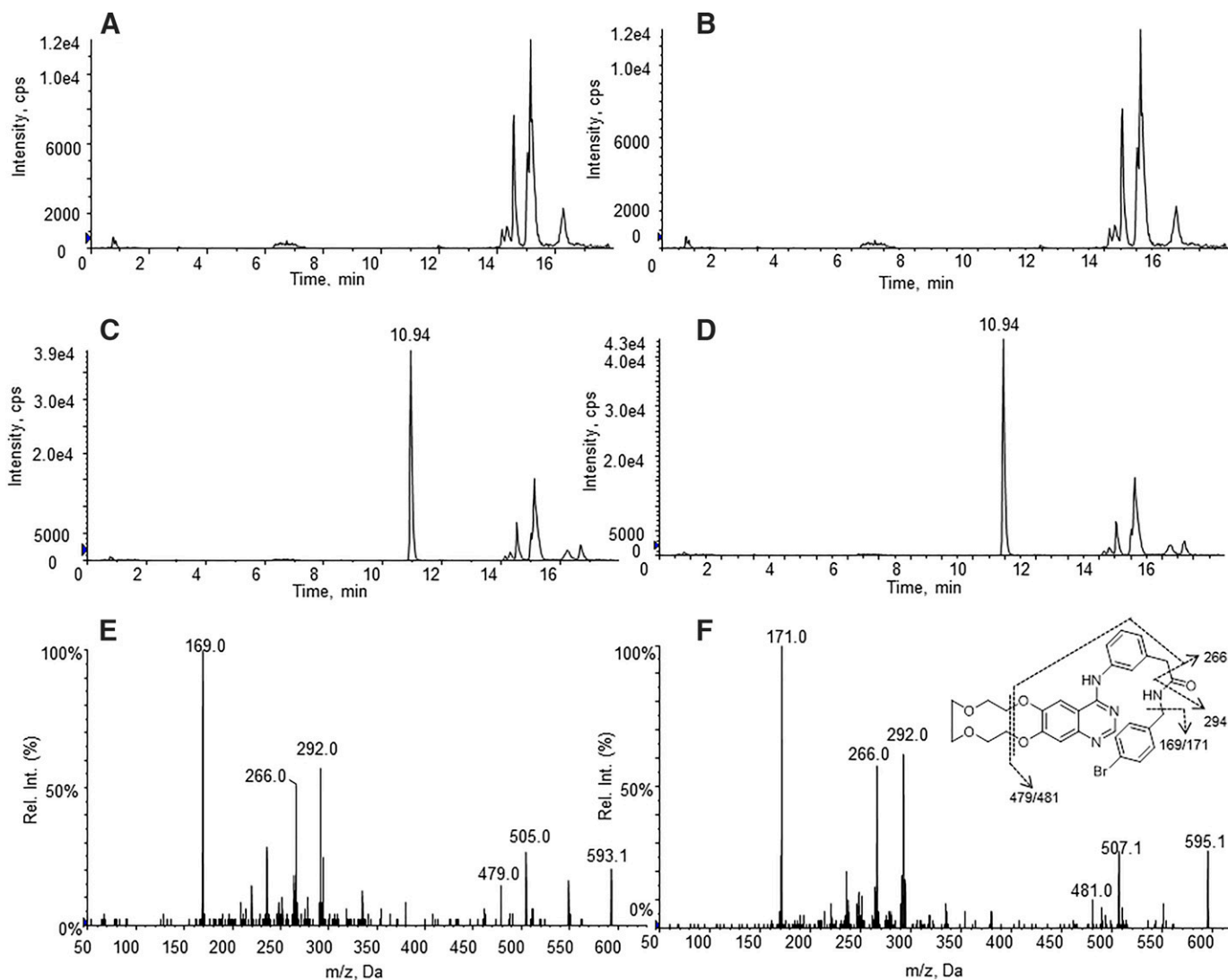
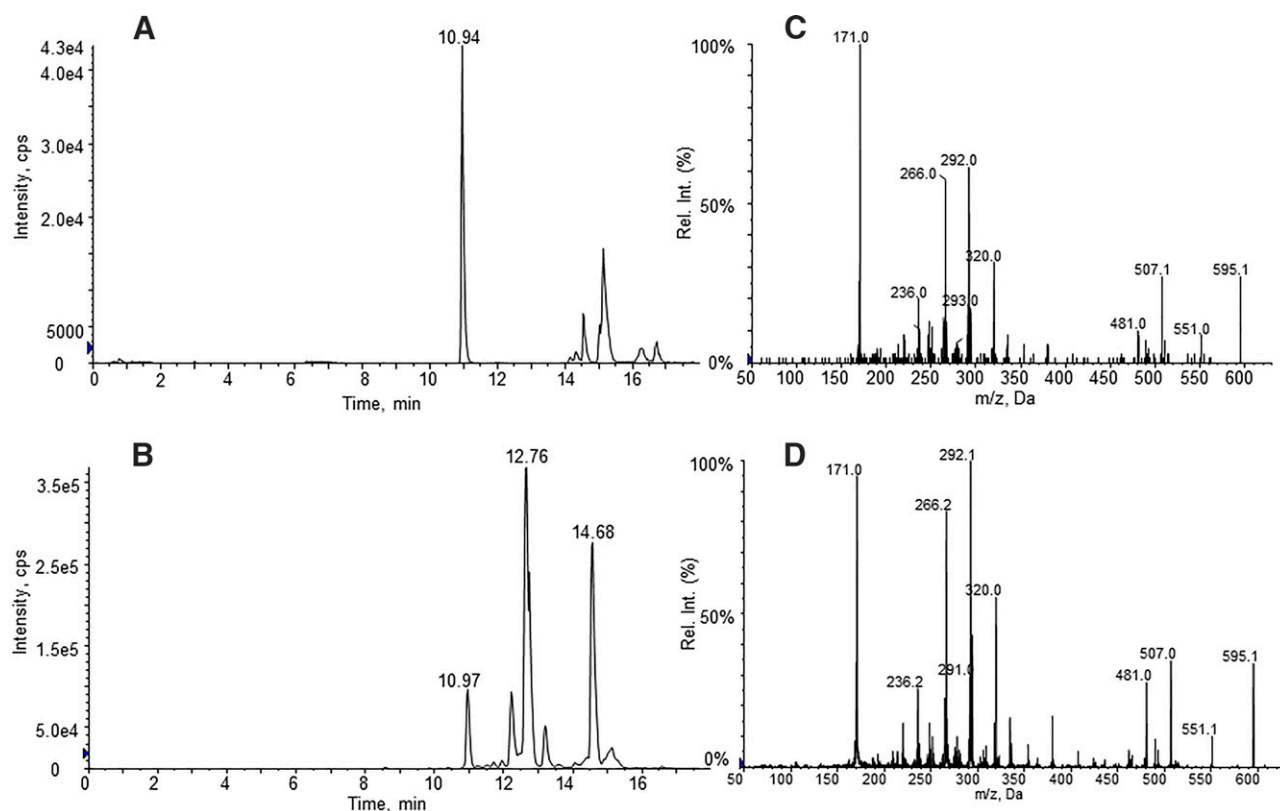


Fig. 6. Identification of ICT-BBA adduct. Ion chromatograms of  $m/z$  593→479 obtained from analysis of human liver microsomes without (A) and with (C) NADPH. Ion chromatograms of  $m/z$  595→481 obtained from analysis of human liver microsomes without (B) and with (D) NADPH. MS/MS spectra obtained from enhanced product ion scanning of ICT-BBA adduct of  $m/z$  593 (E) and 595 (F).





**Fig. 7.** Characterization of synthetic ICT-BBA adduct **5**. Ion chromatograms of  $m/z$  595→481 obtained from analysis of microsomal reactions (A) and biomimetic chemical synthesis (C). MS/MS spectra obtained from enhanced product ion scanning of compound **5** detected in microsomal incubations (B) and biomimetic chemical synthesis (D).

production of ICT-BBA adduct **5**. Figure 9 shows the enzymes involved in the ketene intermediate formation. CYP3A4, followed by CYP2D6 ( $20.9 \pm 3.5\%$  of CYP3A4) and CYP3A5 ( $12.0 \pm 3.6\%$  of CYP3A4) in order of enzyme catalysis efficacy, was the major enzyme participating in the observed bioactivation.

**Changes of the Prosthetic Heme Resulting from Inactivation of CYP3A4 by ICT.** Heme contents of recombinant CYP3A4 after exposure to ICT with or without NADPH were measured to determine

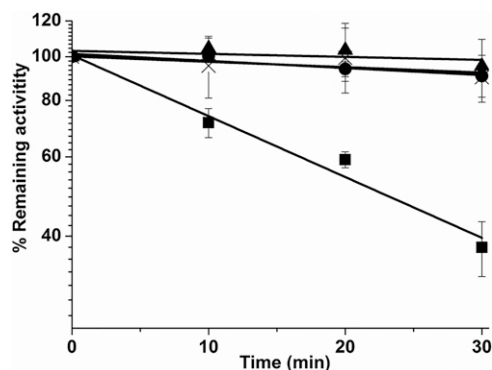


**Fig. 8.** Time-dependent inhibition of CYP3A by ICT and its analogs. NADPH-supplemented human liver microsomes were individually incubated with vehicle (●), ICT (■), analog **2** (■), or analog **3** (×) for 0, 10, 20, and 30 minutes at 37°C and then submitted to CYP3A activity measurement. The resulting enzyme activities examined were calculated by determination of peak area ratio of the analytes versus internal standard. Normalization was established by determination of the enzymatic activity ratio at 0 minutes versus that of each time point. Data represent means  $\pm$  S.D. ( $n = 3$ ).

heme destruction resulting from the metabolic activation of ICT. Internal standard propranolol ( $t_R = 10.39$  minutes; Fig. 10A) enabled us to correct and minimize the errors resulting from instrumental fluctuation and experimental operation. The mass spectrometry response intensity (peak area) of propranolol was consistent in incubations containing ICT and CYP3A4 without (Fig. 10C) or with (Fig. 10E) NADPH. Authentic hemin standard eluted at 13.62 minutes (Fig. 10B), and the MS/MS spectrum of hemin revealed major product ions at  $m/z$  557 and  $[M-CI]^+$  at  $m/z$  616 (quasimolecular ion; Fig. 11). This allowed us to select the ion pair (MRM) to monitor prosthetic heme in incubation mixtures. However, decreased contents of the heme were observed in NADPH-supplemented incubations (Fig. 10F) compared with NADPH-free incubations (Fig. 10D). The peak area ratio of heme to propranolol in NADPH-free incubation fortified with ICT was defined as 100% to determine the involvement of heme in enzyme inactivation. As shown in Fig. 10, incubation of recombinant CYP3A4 with ICT at 50  $\mu$ M for 30 minutes resulted in an approximately 82% decrease in the content of prosthetic heme.

**Interaction of CYP3A4 Apoprotein with Ketene Intermediate.** We also examined the modification of apoprotein by the ketene intermediate using mass spectrometry. Protein obtained from ICT-treated incubation mixture was hydrolyzed by trypsin or chymotrypsin and submitted to LC-MS/MS to determine protein modification. We failed to detect the peptides with an increased molecular weight of 407.148 Da ( $C_{22}H_{21}N_3O_5$ , the mass of ketene intermediate) in positive mode, even with mass tolerance set at 20 ppm (Supplemental Material). Only some unmodified and oxidized peptides from CYP3A4 were detected by LC-MS/MS. This allowed us to exclude the possibility of protein modification as a mechanism for ICT-induced CYP3A inactivation.

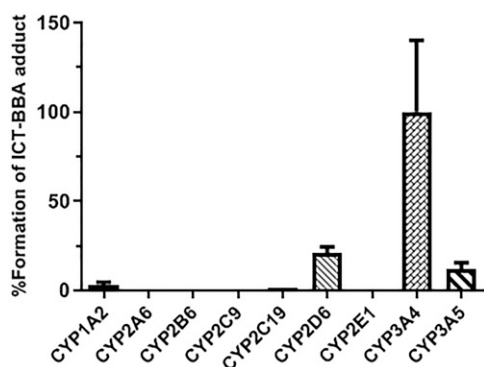


**Fig. 9.** Recombinant human P450s responsible for the generation of the ketene intermediate. ICT was individually incubated with recombinant human P450s supplemented with NADPH and BBA, followed by submitting to LC-MS/MS analysis. The production of ICT-BBA adduct in incubation mixtures of ICT exposed with CYP3A4 was defined as 100% in comparison with that incubated with other recombinant human P450s. Data represent means  $\pm$  S.D. ( $n = 3$ ).

### Discussion

Our study provided, for the first time, the evidence for time-dependent inhibition of CYP3A4/5 by ICT (Fig. 2), with values of  $k_{\text{inact}}$  of  $0.013 \text{ minute}^{-1}$  and  $K_I$  of  $20.8 \text{ }\mu\text{M}$ . ICT-induced CYP3A inactivation was not observed in the incubation mixture without NADPH, indicating that the enzyme inactivation was mediated by biotransformation of P450 enzymes. Mechanism-based inactivation should lie in the metabolic activation of an inactivator precursor and sequential reaction of the host enzyme with the resulting reactive intermediate prior to leaving

the binding pocket. Nifedipine, a substrate of CYP3A, slowed down the CYP3A inactivation induced by ICT (Fig. 3), suggesting that the bioactivation of ICT happened in the active site of CYP3A. Moreover, catalase/SOD did not show protective effects on ICT-induced CYP3A inactivation (Table 1), which enables us to exclude the roles of reactive oxygen species (i.e., superoxide and  $\text{H}_2\text{O}_2$  potentially generated) in the enzyme inactivation. Therefore, the reactive intermediate produced through metabolic activation may be the culprit of the observed mechanism-based inactivation (Kent et al., 2001). GSH and NAL, as nucleophilic agents, were included in incubations for capturing possible reactive electrophilic intermediates that escape from the host enzyme. The incorporation of the nucleophiles failed to reveal protection from the inactivation of CYP3A by ICT (Table 1), which suggests that the reactive metabolite of ICT inactivated the CYP3A prior to releasing from the active site of the enzyme. Meanwhile, the inhibited CYP3A activity was not recovered by dialysis, implying that covalent modification was involved in the enzyme inactivation. Taken together, all evidence points toward the inevitable conclusion that ICT is a mechanism-based inactivator of CYP3A.

CYP3A4 is the major enzyme involved in the metabolism of ICT (Chen et al., 2015). This enzyme is known as the most abundant enzyme of the P450 superfamily in humans, and at least 50% of marketed drugs are metabolized by CYP3A4. Equations for basic models of time-dependent inhibition, according to the relevant U.S. Food and Drug Administration guidance document (Food and Drug Administration, 2020; Vieira et al., 2014), are described in Supplemental Fig. 6. It has been reported that as high as about  $7.5 \text{ }\mu\text{M}$  of plasma  $C_{\text{max}}$  of ICT is circulated in patients given multiple doses (Liu et al., 2015), that the

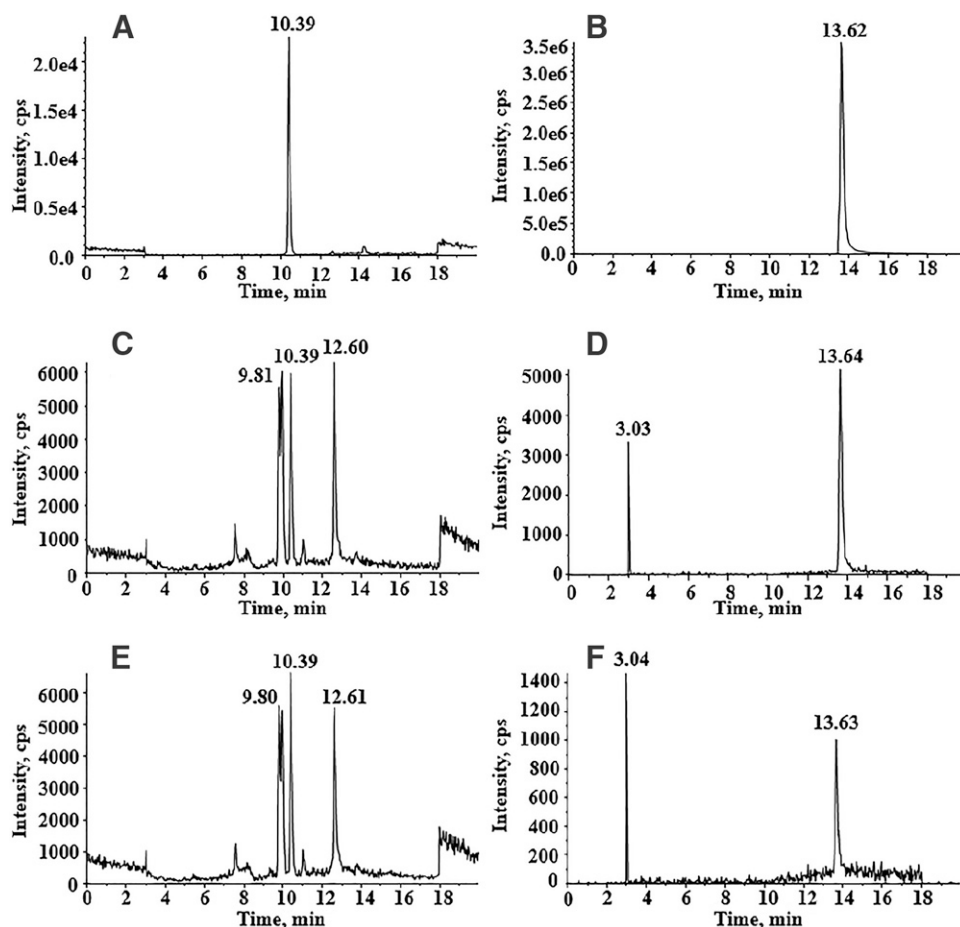
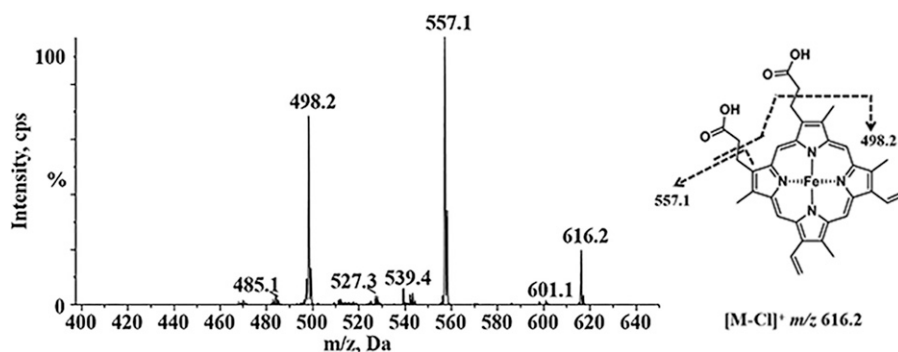


**Fig. 10.** Representative MRM chromatograms for propranolol ( $m/z$  260 $\rightarrow$ 116) (A), (C), (E) and heme ( $m/z$  616 $\rightarrow$ 557) (B), (D), (F) acquired from analyses of propranolol (A), authentic hemin standard (B), and incubation mixtures fortified with ICT and CYP3A4 without [(C) and (D)] or with [(E) and (F)] NADPH.



Fig. 11. MS/MS spectrum of hemin.



human plasma protein binding rate of ICT is around 98.5% (Tan et al., 2009), and that the apparent first-order degradation rate constant of the affected enzyme ( $k_{deg}$ ) is 0.00016  $\text{minute}^{-1}$  (Galetin et al., 2006). For icotinib, the values of  $I_{max,u}$ ,  $K_{obs}$ , and  $R_2$  were 0.1125  $\mu\text{M}$ , 0.0028  $\text{minute}^{-1}$ , and 18.5, respectively, according to the calculation formula mentioned (Supplemental Fig. 6). Since  $R_2 \geq 1.25$ , the DDI potential of icotinib needs further investigation in a clinical DDI study with a sensitive index substrate (Food and Drug Administration, 2020). For example, ritonavir is known as a potent MBI of CYP3A4 (Lim et al., 2005), and the calculated  $R_2$  is 23–26 (Vieira et al., 2014). A study showed that CYP3A remained inhibited 3 days after termination of ritonavir exposure at doses of 300–600 mg daily (Katzenmaier et al., 2011). Ritonavir has been listed as a drug that causes DDI in humans, which is proposed to occur via MBI of CYP3A (Kalgutkar et al., 2007). Like ritonavir, ICT is an MBI of CYP3A with a higher value of  $R_2$  ( $\geq 1.25$ ), which may remind us that DDI may be clinically significant, especially when ICT is coadministered with other medicines with narrow therapeutic windows.

CYP2J2 is another hepatic P450 enzyme, although the content is limited. The enzyme shares similar substrates with CYP3A. We employed nifedipine to probe potential inactivation of CYP2J2 by ICT. Nifedipine is also a mixed inhibitor of CYP2J2 (Ikemura et al., 2019). Mechanistically, a mixed inhibitor is unable to slow down mechanism-based inactivation. Apparently, nifedipine was found to reverse the observed time-dependent inhibition of “CYP3A” (possibly overlapping with CYP2J2 in human hepatic microsomes). If ICT were a mechanism-based inactivator of CYP2J2, such protection effect on the inactivation of “CYP3A” would not have taken place. This enables us to exclude the potential inactivation of CYP2J2 by ICT.

To characterize the role played by reactive intermediates in enzyme inactivation, trapping experiments were performed in human liver microsomal incubations. Trapping agents can be classified as “soft” (GSH/*N*-acetylcysteine) and “hard” (amine derivatives) nucleophiles (Pearson, 1969). A ketene intermediate that is defined as a “hard” electrophile might be formed via the bioactivation of terminal alkyne of ICT. We firstly employed NAL to capture the ketene. Unfortunately, no related adduct was detected (data not shown), possibly resulting from the sensitivity limitation of mass spectrometry. Then we selected BBA, a trapping agent that introduces a bromine in the resulting adduct, for the capture study. BBA, which has been proven to be an effective trapping agent, could be easily cleaved to fragments of  $m/z$  169 and 171 with intensities of 1:1, resulting from 79/81 isotopes of bromine incorporated in mass spectrometric analysis (Wang et al., 2014). This may allow us to avoid a potential false positive, and BBA was successfully employed in trapping *cis*-enedials in our early study (Wang et al., 2014). This did make the mass spectrometry detect the corresponding adduct. We oxidized ICT with *m*-CPBA and reacted

the resulting product with BBA to characterize the adduct. *m*-CPBA is a widely used oxidizing agent in epoxidation reactions. The epoxidation of ICT via biomimetic synthesis using *m*-CPBA to the corresponding oxirene or/and ketene intermediates enables us to mimic the bioactivation of ICT. We speculated that the oxidation of the terminal acetylene by *m*-CPBA offers intermediate **6** (Fig. 5), followed by rearrangement to ketene intermediate **4** and reaction with BBA. In other words, *m*-CPBA mimics the oxidation of the terminal acetylene of ICT catalyzed by P450s. The designed synthetic work allowed us to verify the structure of ICT-BBA adduct **5**, which facilitates the understanding of the metabolic pathway responsible for ICT bioactivation.

Incubation of ICT with the individual recombinant enzymes demonstrated that P450s, such as CYP2D6 and CYP1A2, involved in the generation of the ketene intermediate (Fig. 9), were not necessarily inactivated by the resulting reactive metabolite (data not shown). The explanation for this may result from the absence of nucleophilic amino acid residues in the active site of the metabolizing enzyme. An appropriate distance between the nucleophilic amino acid residue(s) and the reactive intermediate generated in situ is required for covalent binding. This may determine the effectiveness of the enzyme inactivation. Additionally, it is likely that the reactive metabolite escapes from the active site without inactivating the host enzyme (Mao et al., 2018). To further probe the role of the acetylenic group of ICT in the observed CYP3A inactivation, the terminal acetylene of ICT was chemically replaced with a vinyl or ethyl group. The vinyl and ethyl analogs showed no inhibitory effects on CYP3A at all (Fig. 8), indicating the requirement of the acetylenic group for the enzyme inactivation.

In view of the fact that ICT inactivated CYP3A4 more than CYP3A5 and that CYP3A4 was mainly involved in the ketene intermediate formation, we chose CYP3A4 as the enzyme to determine the interaction of reactive metabolites of ICT with the target enzyme. We started with apoprotein adduction investigation by trypsin and chymotrypsin digestion- and LC-MS/MS-based analysis. Unfortunately, mass spectrometric analysis failed to show the evidence for apoprotein modification derived from ICT (Supplemental Material). We then decided to examine the alteration in prosthetic heme content of CYP3A4 incubations with or without exposure to ICT. A dramatic loss (82%) of prosthetic heme content was found in the incubation mixture supplemented with ICT. The observed disappearance of prosthetic heme in ICT-treated CYP3A4 incubation suggests that heme was damaged, resulting from the metabolic activation of ICT. Cytochrome b5 is also potentially alkylated by reactive metabolites resulting in enzyme inactivation (Osawa and Pohl, 1989). Our incubation system did not contain such enzyme, which excludes the participation of cytochrome b5 modification in the observed CYP3A4 inactivation. Together, the finding of heme destruction, along with the failure to detect modified apoprotein, in ICT-treated CYP3A4 indicates that

heme rather than apoprotein was the target of the electrophilic metabolite that participates in the observed enzyme inactivation.

In summary, ICT was proved to be a moderately efficient mechanism-based inactivator of recombinant human CYP3A4/5. Heme destruction by a ketene intermediate biotransformed from the terminal acetylenic moiety of ICT may be responsible for ICT-induced CYP3A inactivation. This study alerts clinicians to be cautious about the potential risk of ICT-induced drug-drug interactions and provides the foundations for the rational design of new drug entities.

#### Authorship Contributions

*Participated in research design:* Sun, Zhao, Peng, Zheng.

*Conducted experiments:* Sun, Zhao, Li, Jia, Yang.

*Performed data analysis:* Sun, Zhao.

*Wrote or contributed to the writing of the manuscript:* Sun, Zhao, Zheng.

#### References

- Bjornsson TD, Callaghan JT, Einolf HJ, Fischer V, Gan L, Grimm S, Kao J, King SP, Miwa G, Ni L, et al. (2003) The conduct of in vitro and in vivo drug-drug interaction studies: a PhRMA perspective. *Drug Metab Dispos* **43**:443–469.
- Blobaum AL, Kent UM, Alworth WL, and Hollenberg PF (2002) Mechanism-based inactivation of cytochromes P450 2E1 and 2E1 T303A by tert-butyl acetylenes: characterization of reactive intermediate adducts to the heme and apoprotein. *Chem Res Toxicol* **15**:1561–1571.
- Campbell L, Blackhall F, and Thatcher N (2010) Gefitinib for the treatment of non-small-cell lung cancer. *Expert Opin Pharmacother* **11**:1343–1357.
- Chen J, Liu D, Zheng X, Zhao Q, Jiang J, and Hu P (2015) Relative contributions of the major human CYP450 to the metabolism of icotinib and its implication in prediction of drug-drug interaction between icotinib and CYP3A4 inhibitors/inducers using physiologically based pharmacokinetic modeling. *Expert Opin Drug Metab Toxicol* **11**:857–868.
- Ciardello F and Tortora G (2001) A novel approach in the treatment of cancer: targeting the epidermal growth factor receptor. *Clin Cancer Res* **7**:2958–2970.
- Food and Drug Administration (2020) *In Vitro Drug Interaction Studies: Cytochrome P450 Enzyme- and Transporter-Mediated Drug Interactions. Guidance for Industry*. Center for Drug Evaluation and Research, U.S. Food and Drug Administration, Silver Spring, MD. Available from <https://www.fda.gov/media/134582/download>
- Foo WY, Tay HY, Chan EC, and Lau AJ (2015) Meclizine, a pregnane X receptor agonist, is a direct inhibitor and mechanism-based inactivator of human cytochrome P450 3A. *Biochem Pharmacol* **97**:320–330.
- Hollenberg PF, Kent UM, and Bumpus NN (2008) Mechanism-based inactivation of human cytochromes p450s: experimental characterization, reactive intermediates, and clinical implications. *Chem Res Toxicol* **21**:189–205.
- Galetin A, Burt H, Gibbons L, and Houston JB (2006) Prediction of time-dependent CYP3A4 drug-drug interactions: impact of enzyme degradation, parallel elimination pathways, and intestinal inhibition. *Drug Metab Dispos* **34**:166–175.
- Gridelli C, Maione P, Bareschino MA, Schettino C, Sacco PC, Ambrosio R, Barbato V, Falanga M, and Rossi A (2010) Erlotinib in the treatment of non-small cell lung cancer: current status and future developments. *Anticancer Res* **30**:1301–1310.
- Gu A, Shi C, Xiong L, Chu T, Pei J, and Han B (2013) Efficacy and safety evaluation of icotinib in patients with advanced non-small cell lung cancer. *Chin J Cancer Res* **25**:90–94.
- Kalgtkar AS, Obach RS, and Maurer TS (2007) Mechanism-based inactivation of cytochrome P450 enzymes: chemical mechanisms, structure-activity relationships and relationship to clinical drug-drug interactions and idiosyncratic adverse drug reactions. *Curr Drug Metab* **8**:407–447.
- Katzenmaier S, Markert C, Riedel KD, Burhenne J, Haefeli WE, and Mikus G (2011) Determining the time course of CYP3A inhibition by potent reversible and irreversible CYP3A inhibitors using a limited sampling strategy. *Clin Pharmacol Ther* **90**:666–673.
- Keating GM (2014) Afatinib: a review of its use in the treatment of advanced non-small cell lung cancer. *Drugs* **74**:207–221.
- Kent UM, Juschyshyn MI, and Hollenberg PF (2001) Mechanism-based inactivators as probes of cytochrome P450 structure and function. *Curr Drug Metab* **2**:215–243.
- Lim HK, Duczak N Jr, Brougham L, Elliot M, Patel K, and Chan K (2005) Automated screening with confirmation of mechanism-based inactivation of CYP3A4, CYP2C9, CYP2C19, CYP2D6, and CYP1A2 in pooled human liver microsomes. *Drug Metab Dispos* **33**:1211–1219.
- Lin HL, Kent UM, and Hollenberg PF (2002) Mechanism-based inactivation of cytochrome P450 3A4 by 17 alpha-ethynylestradiol: evidence for heme destruction and covalent binding to protein. *J Pharmacol Exp Ther* **301**:160–167.
- Liu D, Jiang J, Zhang L, Tan F, Wang Y, and Hu P (2011) Metabolite characterization of a novel anti-cancer agent, icotinib, in humans through liquid chromatography/quadrupole time-of-flight tandem mass spectrometry. *Rapid Commun Mass Spectrom* **25**:2131–2140.
- Liu D, Zhang L, Wu Y, Jiang J, Tan F, Wang Y, Liu Y, and Hu P (2015) Clinical pharmacokinetics, safety, and preliminary efficacy evaluation of icotinib in patients with advanced non-small cell lung cancer. *Lung Cancer* **89**:262–267.
- Mao X, Hu Z, Wang Q, Zhang N, Zhou S, Peng Y, and Zheng J (2018) Nitidine chloride is a mechanism-based inactivator of CYP2D6. *Drug Metab Dispos* **46**:1137–1145.
- McDonald RN and Schwab PA (1964) Strained ring systems. I. Peroxidation studies with certain acetylenes. The relevance of oxirene intermediates. *J Am Chem Soc* **86**:4866–4871.
- Ikemura N, Yamaori S, Kobayashi C, Kamijo S, Murayama N, Yamazaki H, and Ohmori S (2019) Inhibitory effects of antihypertensive drugs on human cytochrome P450 2J2 activity: potent inhibition by azelinidipine and manidipine. *Chem Biol Interact* **306**:1–9.
- Obach RS, Walsky RL, Venkatakrishnan K, Houston JB, and Tremaine LM (2005) In vitro cytochrome P450 inhibition data and the prediction of drug-drug interactions: qualitative relationships, quantitative predictions, and the rank-order approach. *Clin Pharmacol Ther* **78**:582–592.
- Orr ST, Ripp SL, Ballard TE, Henderson JL, Scott DO, Obach RS, Sun H, and Kalgtkar AS (2012) Mechanism-based inactivation (MBI) of cytochrome P450 enzymes: structure-activity relationships and discovery strategies to mitigate drug-drug interaction risks. *J Med Chem* **55**:4896–4933.
- Osawa Y and Pohl LR (1989) Covalent bonding of the prosthetic heme to protein: a potential mechanism for the suicide inactivation or activation of hemoproteins. *Chem Res Toxicol* **2**:131–141.
- Ou SHI (2012) Second-generation irreversible epidermal growth factor receptor (EGFR) tyrosine kinase inhibitors (TKIs): a better mousetrap? A review of the clinical evidence. *Crit Rev Oncol Hematol* **83**:407–421.
- Pearson RG (1969) Hard and soft acids and bases. *Surv Progr Chem* **5**:1–52.
- Regal KA, Schrag ML, Kent UM, Wienkers LC, and Hollenberg PF (2000) Mechanism-based inactivation of cytochrome P450 2B1 by 7-ethynylcoumarin: verification of apo-P450 adduction by electrospray ion trap mass spectrometry. *Chem Res Toxicol* **13**:262–270.
- Ruan CJ, Liu DY, Jiang J, and Hu P (2012) Effect of the CYP2C19 genotype on the pharmacokinetics of icotinib in healthy male volunteers. *Eur J Clin Pharmacol* **68**:1677–1680.
- Shi Y, Zhang L, Liu X, Zhou C, Zhang L, Zhang S, Wang D, Li Q, Qin S, Hu C et al. (2013) Icotinib versus gefitinib in previously treated advanced non-small-cell lung cancer (ICOGEN): a randomised, double-blind phase 3 non-inferiority trial. *Lancet Oncol* **14**:953–961.
- Silverman RB (1995) Mechanism-based enzyme inactivators. *Methods Enzymol* **249**:240–283.
- Stamos J, Sliwowski MX, and Eigenbrot C (2002) Structure of the epidermal growth factor receptor kinase domain alone and in complex with a 4-anilinoquinazoline inhibitor. *J Biol Chem* **277**:46265–46272.
- Tan F, Shen X, Wang D, Xie G, Zhang X, Ding L, Hu Y, He W, Wang Y, and Wang Y (2012) Icotinib (BPI-2009H), a novel EGFR tyrosine kinase inhibitor, displays potent efficacy in pre-clinical studies. *Lung Cancer* **76**:177–182.
- Tan F, Zhang L, Zhao Q, Liu D, Hu Y, Liu Y, Hu Y, Liu Y, Ding L, Hu B et al. (2009) Pharmacology and clinical evaluation of icotinib hydrochloride. *Zhongguo Xin Yao Zazhi* **18**:1691–1694.
- Vieira ML, Kirby B, Ragueneau-Majlessi I, Galetin A, Chien JYL, Einolf HJ, Fahmi OA, Fischer V, Fretland A, Grime K et al. (2014) Evaluation of various static in vitro-in vivo extrapolation models for risk assessment of the CYP3A inhibition potential of an investigational drug. *Clin Pharmacol Ther* **95**:189–198.
- Wang K, Zheng L, Peng Y, Song JE, and Zheng J (2014) Selective and sensitive platform for function-based screening of potentially harmful furans. *Anal Chem* **86**:10755–10762.
- Wang W, Song Z, and Zhang Y (2017) Zoledronic acid as potential efficacy application combined with icotinib for non-small cell lung cancer with bone metastases. *Transl Cancer Res* **6**:129–135.
- Yamreudeewong W, DeBisschop M, Martin LG, and Lower DL (2003) Potentially significant drug interactions of class III antiarrhythmic drugs. *Drug Saf* **26**:421–438.
- Zhao Q, Wang Y, Tang Y, and Peng L (2014) Icotinib combined with rapamycin in a renal transplant recipient with epidermal growth factor receptor-mutated non-small cell lung cancer: a case report. *Oncol Lett* **7**:171–176.
- Zhao Y (2017) Feilui decoction combined with icotinib tablets in the treatment of advanced lung cancer 30 cases. *Guangming J Chin Med* **32**:2244–2245.

**Address correspondence to:** Dr. Jiang Zheng, Wuya College of Innovation, Shenyang Pharmaceutical University, Shenyang, Liaoning, 110016, People's Republic of China; State Key Laboratory of Functions and Applications of Medicinal Plants, Guizhou Provincial Key Laboratory of Pharmaceuticals, Guizhou Medical University, Guiyang, Guizhou, 550004, People's Republic of China. E-mail: zhengneu@yahoo.com; or Dr. Ying Peng, Wuya College of Innovation, Shenyang Pharmaceutical University, PO Box 21,103 Wenhua Road, Shenyang 110016, People's Republic of China. E-mail: yingpeng1999@163.com